Synthesis and Characterization of modified PLZT ceramics

Dissertation submitted in partial fulfillment for the requirement of the award of the degree of

Master of Science
In
PHYSICS

Under
The supervision of
Dr. Poonam Uniyal
(Assistant Professor)

Submitted by
Manpreet kaur
Roll no: - 301004006

School of Physics and Materials Science
Thapar University
Patiala (Punjab) – 147004
July, 2012

Certificate

This is to certify that **Miss Manpreet Kaur** has worked on this thesis report entitled "**Synthesis and Characterization of modified PLZT ceramics**" in partial fulfillment of the requirement for the award of degree of Master of Science in Physics in Thapar University, Patiala. This report is authentic record of her own work carried out under the supervision of **Dr. Poonam Uniyal**. The matter embodied in this report is one of the candidate's own record and not submitted to any other University in any part or full form for the award of such kind of degree.

(Dr. Poonam Uniyal)
Supervisor
School of Physics and Material Science
Thapar University
Patiala, INDIA

Countersigned by:

Dr. Kulvir Singh
Professor and Head
School of Physics and Material Science
Thapar University
Patiala, INDIA

(Dr. S.K. Mohanpatra)
Dean of academic affairs
Thapar University
Patiala, INDIA

Acknowledgment

I express my deep sense of gratitude and respect to my guide **Dr. Poonam Uniyal, Assistant Professor, School of Physics and Material Science, Thapar University, Patiala,** for her keen interest and valuable guidance, strong motivation and constant encouragement during the course of the work. I thank her from the bottom of my heart for introducing me to fundamentals of Condensed matter physics. I am sure that the knowledge gained through my association under her supervision shall help me to realize my goals in life.

My sincere thanks to **Dr. Kulbir Singh,** Professor and Head, School of Physics and Material Science for his talented advice and providing necessary facility for my work.

My sincere thanks to Professor **K. K. Raina** for providing his lab facilities especially for dielectric measurements and also to his research Scholar **Ravi Shukla** who helped in taking measurements.

I am especially indebted to **Dr. K. L. Yadav** (IIT Roorkee) for providing his lab facilities for sample preparations, without his help the sample preparation would not have been possible.

I am also thankful to all research scholars specially **Mrs. Nandini** for their kind support, help and time to time discussion.

I would like to express my gratefulness to my brother **Amritpal Singh** and friend **Vipul Anand** for their endless support, without which I could not complete my project work.

Finally, I would like to express my deepest gratitude to **my parents**, without whom I am nothing, to provide me great opportunities, everlasting support, big encouragement and lots of love.

Manpreet Kaur

(*Manpreet kaur*)

List of Figures and Tables

List of Symbols

θ	Angle
A	Area
E_c	Coercive field strength
C	Curie constant
C_P	Capacitance
T_o	Curie temperature
K	Dielectric constant
$\tan\delta$	Dielectric loss
d	Distances
δ	Diffuse coefficient
γ	Diffusivity
E	Electric Field
L	Inductance
n	Integer
$\prod$	Pyroelectric coefficient
P	Polarization
ε	Permittivity of material
ε_0	Permittivity of vacuum
P_r	Remnant polarization
C_0	Reference capacitor
ε_r	Relative permittivity
R	Resistance
P_s	Spontaneous polarization
P_{sat}	Saturation value
T	Temperature
T_c	Transition temperature
t	Thickness
λ	Wavelength

Abstract

Polycrystalline samples of Dy modified lead Zirconate titanate $Pb_{0.92}La_{0.08}(Zr_{0.65}Ti_{0.35})O_3$ (PLZT) was prepared by the conventional method based on the solid state reaction of mixed oxides. The structural characterization of the samples investigated by X-ray diffraction technique exhibited rhombohedral structure. PLDZT (65/35) ceramics show single perovskite phase. Scanning electron micrographs was employed to study the Microstructure. Detailed Dielectric study was done in the temperature range of 30^0C to 400^0C in the frequency range of 100 Hz to 1MHz.

Contents

Chapter:1 Introduction to ferroelectricity

Chapter:2 Motivation for work

Chapter:3 Synthesis and Experimental techniques

Chapter: 4 Results and discussion

Chapter: 1

Introduction to Ferroelectricity

In the recent years, Polymer composite materials have been widely used because of their significant importance. Now the research is rapidly going on ferroelectric composite material because of their various applications due to their excellent properties. J.Valasek [1], who was investigating the dielectric properties of Rochelle salt ($NaKC_4H_4O_6.4H_2O$), discovered the phenomenon of ferroelectricity in 1921. There are more than 250 materials that exhibit ferroelectric properties. Barium titanate ($BaTiO_3$), Lead titanate ($PbTiO_3$), Lead zirconate titanate (PZT) and Lead lanthanum zirconate titanate (PLZT) are some of the more common/significant ferroelectric materials.

1.1 Ferroelectricity

Ferroelectricity is the occurrence of a spontaneous electric polarization in a crystal in the absence of an external field. By the application of an external electric field, the spontaneous polarization can be reversed. It is an intrinsic property of the crystal. Some Ferroelectric properties are:

1.1.1 Spontaneous Polarization and Pyroelectric Effect

In the certain range of temperature, the material becomes spontaneously polarized, i.e., an electric polarization develops in it without the help of external field (This phenomenon is analogous to the spontaneous magnetization which takes place in ferromagnetic materials.).

The axis of spontaneous polarization is usually along a given crystal axis. Although a crystal with polar axes (20 non-centrosymmetric point groups) shows the piezoelectric effect, it is not necessary for it to have a spontaneous polarization vector. It could be due to the canceling of the electric moments along the different polar axes to give a zero net polarization. Only crystals with a unique polar axis (10 out of 21 non-centrosymmetric point groups) show a spontaneous polarization vector P_s along this axis.

In some crystals the ferroelectric dipole moment is not changed by an electric field of the maximum intensity which is possible to apply before causing electrical breakdown. In these crystals we are often able to observe a change in the spontaneous moment when the temperature is changed. Such crystals are called the pyroelectric crystals. First pyroelectric crystal, tourmaline was discovered by Teophrast in 314 B.C. and so named by Brewster in 1824 [2]. The pyroelectric effect can be described in terms of the pyroelectric coefficient $\prod$. A small change in the temperature ΔT, in a crystal, in a gradual manner, leads to a change in the spontaneous polarization vector ΔP_s given [3] by,

$$\Delta P_s = \prod \Delta T \qquad \ldots [1.1]$$

1.1.2 Ferroelectric Domains and Hysteresis Loop

Ferroelectric crystals possess regions with uniform polarization called ferroelectric domains. Within a domain, all the electric dipoles are aligned in the same direction. The net polarization depends on the difference in the volumes of the upward and downward-directed domains. There may be many domains in a crystal separated by interfaces called domain walls. A ferroelectric single crystal, when grown, has multiple ferroelectric domains, as shown in Figure 1.1.

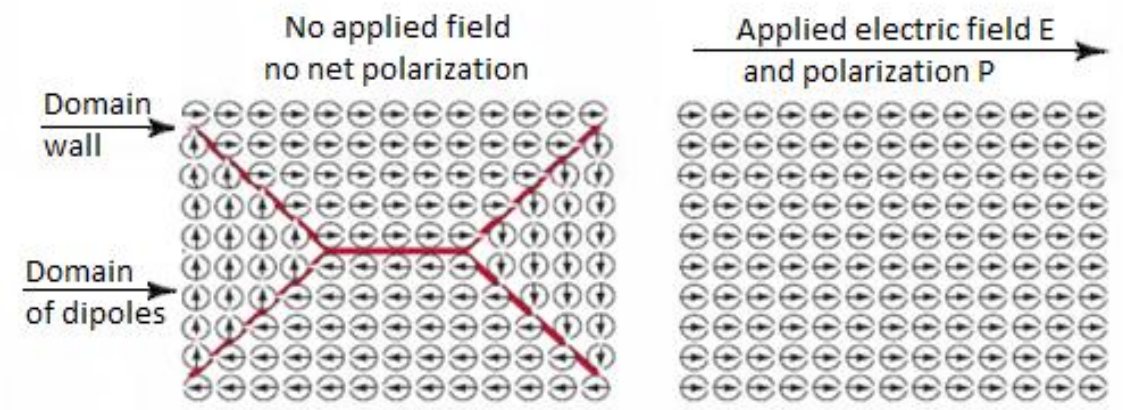

Figure: 1.1. Schematic of the poling process in piezoelectric ceramics: **(a)** In the absence of electric field the domains have random orientation of polarization; **(b)** The polarization within the domains aligns in the direction of the applied field.

A single domain can be obtained by domain wall motion, which can be made possible by the application of an appropriate electric field. A very strong field could lead to the reversal of the polarization in the domain [4, 5].

A Polarization vs. Electric Field (P-E) hysteresis loop for a typical ferroelectric crystal is shown in Figure 1.2. When the electric field strength increases, then all the domains start to align in the positive direction. It will give rise to a rapid increase in the polarization (OB). As the strength of electric field rises to a very high level, the polarization reaches at a saturation value P_{sat}. If the external field is removed, the polarization does not fall to zero. At zero external field, some of the domains remain aligned in the positive direction, hence the crystal will show a remnant polarization P_r. The crystal cannot be completely depolarized until a field of magnitude (OF) is applied in the negative direction. An external electric field is required to reduce the polarization to zero, that external field is called the coercive field strength E_c. If the external electric field is increased to a more negative value, the direction of polarization flips and hence a hysteresis loop is obtained. The value of the spontaneous polarization P_s (OE) is obtained by extrapolating the curve onto the polarization axes (CE).

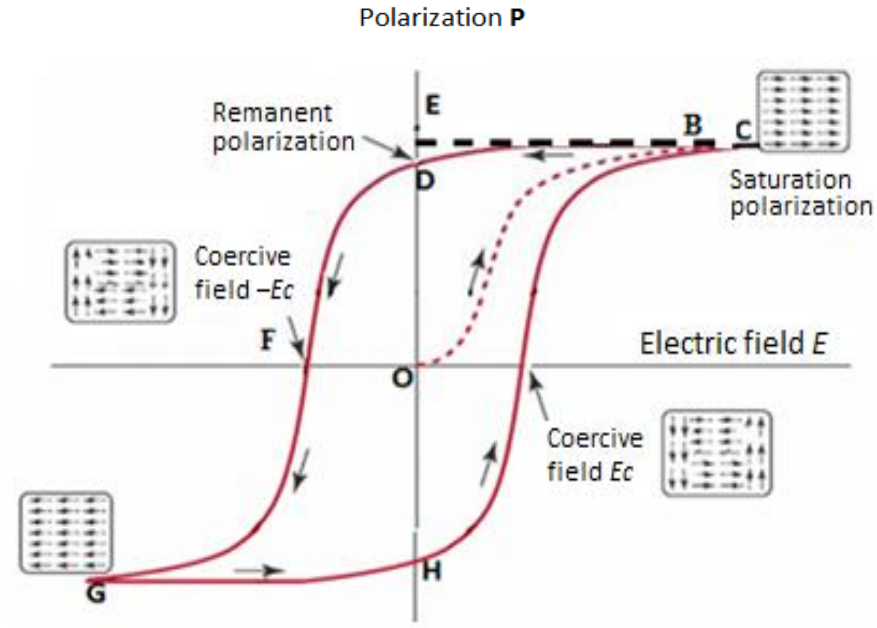

Figure: 1.2. A Polarization vs. Electric Field (P-E) hysteresis loop for a typical ferroelectric crystal. [6]

1.1.3 Curie point and Phase Transitions

Curie point (T_c) is the transition temperature for all the ferroelectric materials. The crystal does not exhibit ferroelectricity when the temperature $T > T_c$, while for $T < T_c$ it is ferroelectric. When temperature goes down through the Curie point, a phase transition from non-ferroelectric phase to a ferroelectric phase happens in the ferroelectric crystal. It consists of one and more than one ferroelectric phases. If it shows more than one ferroelectric phases, the crystal transforms from one ferroelectric phase to another at a temperature. That temperature is known as transition temperature. Some of the ferroelectric transitions in $BaTiO_3$ have been summarized by Nettleton [7, 8]. Figure 1.3 shows the variation of the relative permittivity ε_r with temperature as a $BaTiO_3$ crystal is cooled from its paraelectric cubic phase to the ferroelectric tetragonal, orthorhombic, and rhombohedral phases.

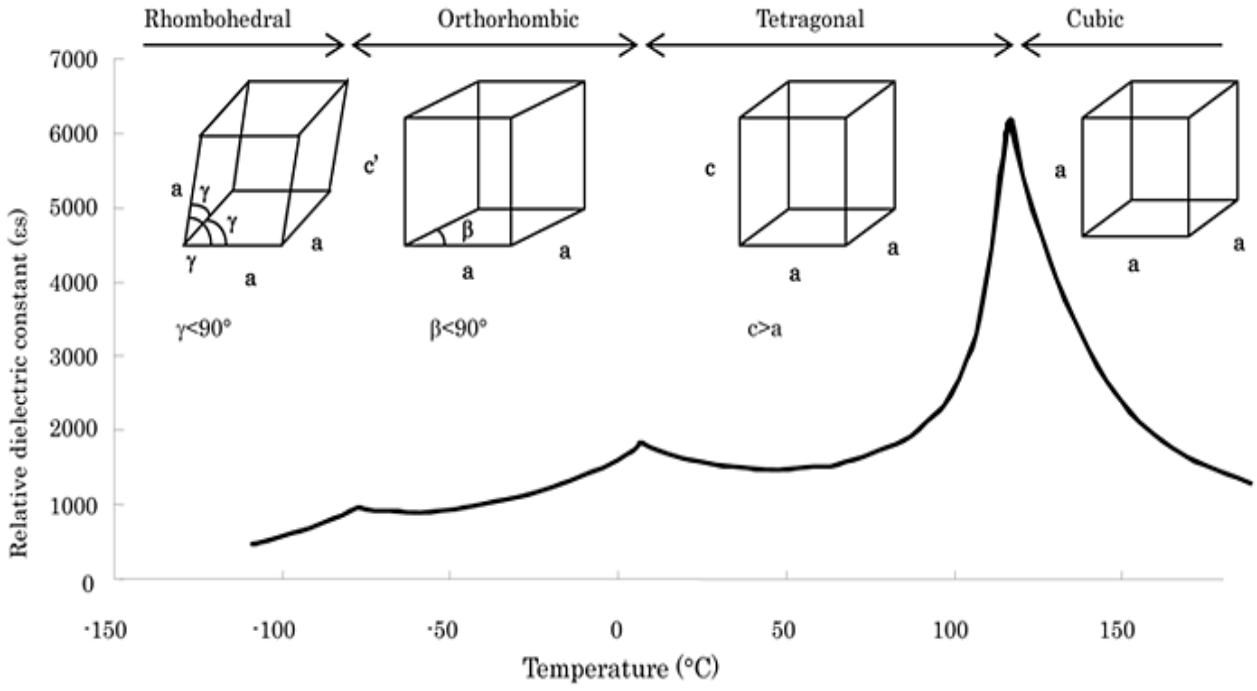

Figure: 1.3. The variation of the relative permittivity ε_r with temperature (pure $BaTiO_3$) [9].

All the thermodynamic properties including dielectric, elastic, optical, and thermal constants show an anomalous behavior near the Curie point or say transition temperatures. This anomalous behavior comes into picture because of the distortion in the crystal as the phase structure changes. The temperature dependence of the dielectric constant above the Curie point ($T > T_c$) in ferroelectric crystals is governed by the [10] Curie-Weiss law:

$$\varepsilon = \varepsilon_0 + C/ (T-T_o) \quad \ldots [1.2]$$

where "ε" is the permittivity of the material, "ε_0" is the permittivity of vacuum; "C" is the Curie constant and "T_o" is the Curie temperature. As we know that Curie temperature T_o is not same as the Curie point T_c, both are quite different. T_o is a formula constant obtained by extrapolation, while T_c is the actual temperature where the crystal structure changes. For first order transitions $T_o < T_c$ while for second order second order phase [11] transitions $T_o=T_c$.

1.2 Applications of ferroelectric materials

- Capacitors
- Light deflectors, modulators and displays
- Piezoelectrics for ultrasound imaging and actuators
- Electro-optic materials for data storage applications
- Thermistors
- Switches known as transchargers or transpolarizers
- Oscillators and filters
- Non-volatile memory

1.3 Structural Classification of Ferroelectric Materials

Ferroelectric crystals have been grouped together according to their major four different structures:

- Perovskite Structure
- Tungsten Bronze Structure

- Bismuth Oxide layer Structure
- Lithium Niobate and Tantalate Structure

We generally use perovskite structure of material because it shows excellent Dielectric properties.

1.4 Lead Zirconate Titanate (PZT)

Lead Zirconate Titanate (PZT) with the common formula (Pb [Zr_x $Ti_{(1-x)}$] O_3) is a binary solid solution of $PbZrO_3$ (an antiferroelectric) and $PbTiO_3$ (a ferroelectric). Figure 1.4 shows a unit cell of PZT. In PZT, the chemical elements are lead and zirconium and the chemical compound titanate which are combined under extremely high temperatures. PZT has a perovskite crystal structure in which each unit consists of a small tetravalent metal ion in a lattice of large divalent metal ions. The large divalent metal ion is usually lead. Under conditions that confer a tetragonal or rhombohedral symmetry on the PZT crystals, each crystal has a dipole moment.

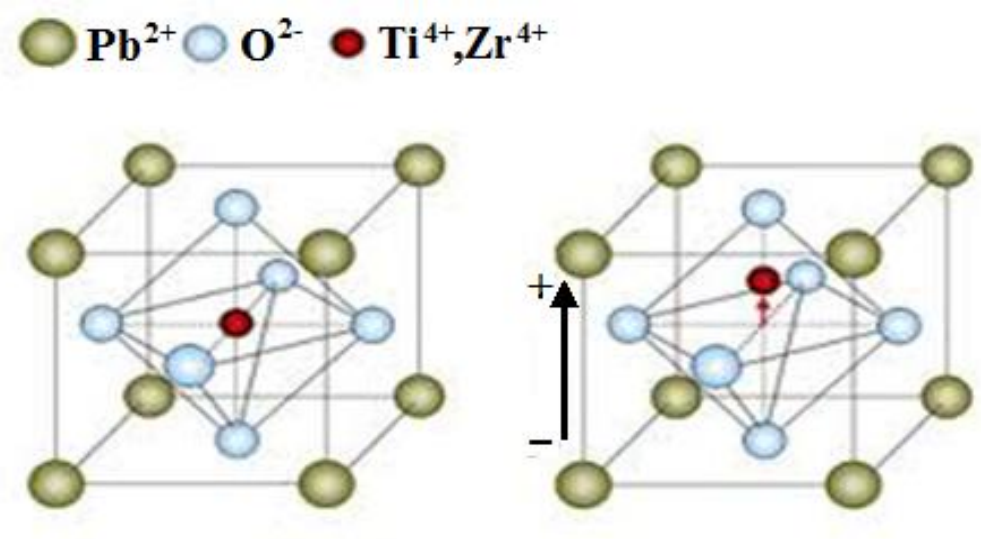

Figure: 1.4. Structural representation of PZT

In the idealized cubic unit cell of such a compound, 'Pb^{2+}' atom sits at cube corner positions (0, 0, 0), 'Ti^{4+}, Zr^{4+}' atom sits at body centre position (1/2, 1/2, 1/2) and oxygen atoms sit at face

centered positions (1/2, 1/2, 0). The diagram shows edges for an equivalent unit cell with Pb^{2+} at the corners, Ti^{4+}, Zr^{4+} in body centre, and O^{2-} in mid-edge.

1.4.1 PZT Properties

PZT compound is the one of the most prominent and useful electro-ceramic because of its properties. It shows the piezoelectric behavior, when a high voltage or potential difference across two of its faces or by applying the external field it changes its physical shape. The dielectric constant of PZT ceramic (ranges from 300 to 3850) depending upon the orientations and doping. Because of this it can used in sensor and actuator applications. They also show the pyroelectric behavior i.e., the material develops a voltage difference across two of its faces when it experiences a temperature change. As a result, it can be used as a sensor for detecting heat. It is also a ferroelectric, which means it has a spontaneous electric polarization (electric dipole) which can be reversed in the presence of an electric field.

Table: 1.1. Some important values of PZT

Materials	Dielectric Constant ε_r	Remnant Polarization P_r ($\mu C/cm^2$)	Curie Temperature T_c (^0C)
PZT	1,000-4,100	3.6	170-360

1.5 Dielectric constant (K) and dielectric loss (tanδ)

The relative dielectric constant K is the ratio of the permittivity ε of the material and the permittivity of free space ε_0 ($8.85x10^{-12}F/m$). Room temperature capacitance C_P and dielectric loss (tanδ) were measured using multi frequency LCR meter (Model-FLUKE PM6306, programmable automatic LCR meter). Dielectric constant K was calculated from the measured capacitance using equation [1.3].

Room temperature dielectric measurements were done for the electroded pellets.

$$K = \varepsilon/\varepsilon_0 \text{ and } \varepsilon = C_p \times (t/A) \quad \ldots [1.3]$$

Where ε is the permittivity of the material, ε_0 the permittivity of free space, C_P the capacitance, t the thickness, and A the area of pellets.

Dielectric permittivity is a complex value. Under the application of alternating voltage it has both real (in phase) and imaginary (out of phase) components.

$$\varepsilon = \varepsilon' + i\varepsilon'' \quad \ldots [1.4]$$

Dielectric loss (D or tanδ) is the ratio of imaginary and real components, and expressed by simple mathematical equation [1.5].

$$\tan\delta = \varepsilon''/\varepsilon' \quad \ldots [1.5]$$

Chapter: 2

Motivations for Work

Motivation

Lead-based perovskite ferroelectric ceramics are widely applied in multilayer capacitors, micro-electro mechanical systems (MEMS) and integrated devices such as ferroelectric memories, infrared sensors, micro actuators, etc. [12-15]. Many of these applications demand materials with excellent dielectric and ferroelectric properties. Lead zirconium titanate (PZT) is one of the best lead-based materials that have been studied extensively since late 1940s [16, 17]. The dielectric characteristics of PZT ceramic are changes with its stoichiometry [18].

PZT is an ABO_3 type perovskite structured material with A-site (Pb^{2+}) occupying cubo-octohedral interstices described by the BO_6 site octahedral and has tetragonal, rhombohedral and orthorhombic phases at room temperature, depending on the value of Zr/Ti ratio. It has two morphotropic boundaries (MPB) at 95/5 and 53/47 Zr/Ti ratio[19], where it undergo phase transition from orthorhombic to low temperature rhombohedral and high temperature rhombohedral to tetragonal phases, respectively. All these compositions show cubic phase above transition temperature. The composition near MPB region normally shows an increased capability of polarization and electromechanical response, which make them suitable for non-volatile memories and piezoelectric actuators [20-22].

PZT compositions show significant merit, when they are doped with foreign ions. Its dielectric and piezoelectric properties change, depending on the site occupied by the foreign ion in ABO_3 perovskite structure. Dopants are classified as Isovalent, acceptors or donors [23].

Donors (trivalent ion at A site and pentavalent ion at B site) reduce the concentration of intrinsic oxygen vacancy created due to PbO evaporation and compensate the hole formed due to lead vacancies, which in turn increases bulk resistance of sample.

Acceptors (monovalent at A site and trivalent at B site) introduce oxygen vacancies to maintain charge neutrality, due to this oxygen vacancy domain walls gets pinned and space charges are introduced, which in turn reduces grain resistance and inhibits domain motion [24],

also acceptor-doped PZT shows poor hysteresis loop and low dielectric constant. Isovalent (divalent at A site and tetravalent at B site) doping tends to reduce the Curie temperature [20] and increases the density of PZT ceramic, which in turn effect the electrical properties. A list of more commonly used dopants is given in Table 2.1

Table: 2.1 List of common ion substitution in PZT

Pb site donors La^{3+}, Bi^{3+}, Nd^{3+}, Sb^{3+}, Th^{4+}
Ti–Zr site donors Nd^{5+}, Ta^{5+}, Sb^{5+}, W^{6+}
Pb site acceptors K^{+}, Na^{+}, Rb^{+}
Ti–Zr site acceptors Fe^{3+}, Al^{3+}, Sc^{3+}, In^{3+}, Cr^{3+}, Co^{3+}, Ga^{3+}, Mn^{3+}, Mg^{2+}, Cu^{2+}
Isovalent substitutions Sr^{2+}, Ca^{2+}, Ba^{2+}(for Pb^{2+}) Sn^{4+} (for Ti^{4+}, Zr^{4+})
Multivalent ions Cr, U

The double doping is carried out in PZT (65/35) with a common formula of $Pb_{0.92}(La_{1-x}A_x)_{0.08}(Zr_{0.65}Ti_{0.35})_{0.98}O_3$, where A = Na [26], K [27], Cs [28], Bi [29], Ca [30], Eu [31] and Fe [25], and their effects on structural, dielectric, optical, ferroelectric, pyroelectric and piezoelectric properties were investigated. Dutta *et al* substituted Fe^{3+} in the La site and found that the transition temperature shifts to a higher temperature with Fe doping with increasing dc and ac conductivities showing semiconductor behavior. The impedance analysis carried out by the same group found the presence of non-Debye type multiple relaxations [32].

Ramam and Lopez have replaced Fe^{3+} at the B site and reported that the remanent polarization and saturation polarization reach saturation at 6 mol% Fe, while the coercive field saturated at 3 mol% Fe along with a decreasing trend of piezoelectric parameters [33]. In this work we have replaced Fe^{3+} at the Pb^{2+} site and studied its effect on the structural, dielectric, ferroelectric and pyroelectric properties. Also the impedance analysis was carried out to study the grain boundary resistance of Fe doped PLZT ceramics.

In PLZT ceramics, the common formula considered is $Pb_{0.92-x}La_{0.08}Dy_x(Zr_{0.65}Ti_{0.35})_{1-x/4}V(B)_{x/4}O_3$, where V(B) signifies vacancies at the B site. It has been shown by Hardtl that if the doped ion contains a valency higher than that of the host ion substituted (Dy^{3+} at the Pb^{2+} site or the trivalent ion at the A site), the vacancies occur in the cation sublattice [34]. Conversely, if the doped ion contains a valency lower than that of the host ion substituted (Fe^{3+} at the Ti^{4+} site or the trivalent ion at the B site), then the vacancies are found to occur at the anion sublattice. Nevertheless, it has been observed by Hardtl and Hennings [35] that the vacancies can be found in both A and B sites of the PLZT lattice.

Radheshyam Rai *et al* have suggested that the substitution of La^{3+} at Pb site of PZT (PLZT) gives improved optoelectric and piezoelectric properties of materials. PLSZT compound indicates the sharp and single diffraction peaks and of single phase with tetragonal structure. They suggest that there is no change in the basic crystal structure of PLZT on substitution of Sb. Some changes in the intensity have been observed due to variation in particle size and presence of Sb. At the frequency of 10 kHz, the peak dielectric permittivity increases with the increase of concentration of Sb and resistivity was found to increase [36].

Soma Dutta *et al* observed that substitution of Bi^{3+} in PLZT have the monophasic rhombohedral structure. The calcined PLBZT powders shows that the particles are spherical and well dispersed with an average size of about 16-18 nm. Dielectric peaks are found to be broadened and shifts towards the high temperature side with increasing Bi^{3+} contents [38]. Grain size was decreasing due to doping. All the Bi-rich PLBZT compounds are of good thermal stability and decrease in piezoelectric coefficient due to incorporation of Bi in PLZT [37].

To the best of our knowledge no work has been done on PLDZT ceramics till date. In the present work, we have synthesized Dy doped PLZT samples and studied the electrical properties.

Chapter: 3

Synthesis and Experimental techniques

3.1 Solid state reaction method

Polycrystalline samples of $Pb_{0.92-x}La_{0.08}Dy_x$ $(Zr_{0.65}$ $Ti_{0.35})_{1-x/4}O_3$ (PLDZT) with (x = 0.0 and 0.03) were synthesized from high purity oxides. As starting materials PbO, TiO_2, La_2O_3, ZrO_2 and Dy_2O_3 were used. All the constituent compounds were thoroughly mixed in an agate mortar for 2h in suitable stoichiometry. After mixing, the mixed materials were then calcined at 1000^0C for 4 h. The process of grinding and calcination was repeated till a homogeneous fine powder of the desired compound was obtained. The calcined fine powder was cold pressed into cylindrical pellets of size 8mm diameter and 1–2mm thickness using a hydraulic press at a pressure of 31.2×10^6 Pa.

The pellets were sintered in the PZ atmosphere at 1100 ^{0}C for 2 h. The formation and quality of compounds were checked by the XRD technique. The x-ray diffraction pattern of the compounds was recorded at room temperature using an x-ray powder diffractometer (Brueker D8 Advance) with Cu K_α radiation (1.5418 Å) in a wide range of Bragg angles 2θ(20^0–60^0) at a scanning rate of 2^0 min^{-1}. The flat polished surface of the sintered pellets was the electroded with air drying silver paste and fired at 120 ^{0}C for 30 min before taking electrical and dielectric measurements. The dielectric constant (ε) and loss tangent (tan δ) of the compounds were measured using an automated Model-FLUKE PM6306, programmable automatic LCR meter capacitance measuring assembly as a function of frequency (100 Hz–100 kHz) in the temperature range 40–300 ^{0}C. The polarization–electric field (P–E) hysteresis loops were carried out at room temperature by the modified Sawyer–Tower circuit (Automatic PE loop tracer system, Marine India Electr. Pvt. Ltd).

To understand the structural, electrical properties of the material used different characterization methods.

3.2 X-Ray Diffraction (XRD)

X-ray powder diffraction (XRD) is a versatile, non-destructive technique that reveals detailed information about the chemical composition and crystallographic structure of natural and synthesized materials. It can also provide the dimensional information on unit cell. The analyzed material is finely ground, homogenized, and average bulk composition which is determined. The XRD apparatus is shown in the figure 3.1.

The XRD is an efficient analytical technique used to identify and characterize unknown crystalline materials. Monochromatic X-rays are used to determine the interplanar spacing of the unknown materials. Samples are analyzed as powders with grains in random orientations to ensure that all crystallographic directions are "sampled" by the beam. When the Bragg conditions for constructive interference are obtained, a "reflection" is produced, and the relative peak height is generally proportional to the number of grains in a preferred orientation.

Figure: 3.1. Overview of the XRD apparatus

Bragg's law:

Figure 3.2. shows, when a crystal is bombarded with X-rays of a fixed wavelength and at certain incident angles, intense reflected X-rays are produced when the wavelengths of the scattered X-rays interfere constructively. In order for the waves to interfere constructively, the differences in the travel path must be equal to integral multiples of the wavelength. When this constructive interference occurs, a diffracted beam of X-rays will leave the crystal at an angle equal to that of the incident beam. To illustrate this feature, consider a crystal with crystal lattice planar distances "d".

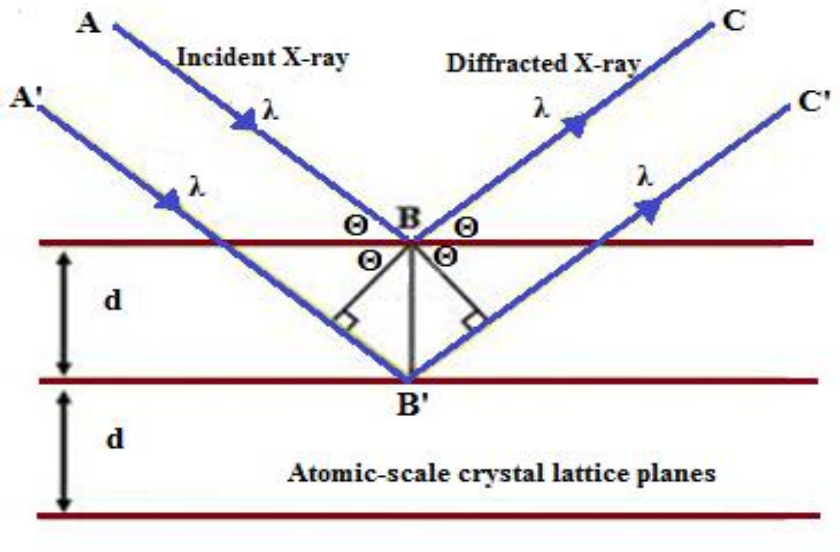

Figure: 3.2. Schematic for Bragg's law

where the travel path length difference between the ray paths of two beams (ABC and A'B'C') is an integral multiple of the wavelength, constructive interference will occur for a combination of that specific wavelength, crystal lattice planar spacing and angle of incidence (θ). Each rational plane of atoms in a crystal will undergo refraction at a single, unique angle (for X-rays of a fixed wavelength).According to Bragg's Law.

i.e.

$$2\,d\,\mathrm{Sin}\,\theta = n\lambda \qquad \ldots [3.1]$$

where n is an integer that indicates the order of reflection, λ is the wavelength of the incident X- rays, d is the inter-planar spacing of the crystal and θ is the angle of incidence.

3.3 Scanning Electron Microscopy (SEM)

The electron column, sample chamber, EDS detector, electronics console, and visual display monitors, all are including in a typical SEM instrument. The scanning electron microscope generates a variety of signals at the surface of solid specimens by using a focused beam of high-energy electrons. The signals that derive from electron-sample interactions reveal information about the sample including external morphology (texture), chemical composition, crystalline structure and orientation of materials making up the sample. In most of the applications, data are collected over a selected area of the surface of the sample. A spatial variation is displayed in these properties when 2-dimensional image is generated. Using conventional SEM techniques, Areas (ranging from approximately 1 cm to 5 microns in width) can be imaged in a scanning mode. SEM is also used to perform analysis of point locations on the sample which are very useful especially in determining chemical compositions, crystalline structure, and crystal orientations qualitatively or semi-quantitatively.

3.3.1 Scanning process and image formation of SEM

In the process of SEM, the tungsten filament cathode is fitted with an electron gun which emits the thermionically an electron beam. Tungsten is mainly used in thermionic electron guns because of its best properties. Those properties are: it is very cheap, it has the highest melting point and it also has the lowest vapour pressure of all metals because of this property. There are two condenser lenses which are focused on an electron beam, ranging from 0.2 keV to 40 keV, to a spot of about 0.4 nm to 5 nm in diameter.

To scan the sample, the beam passes through the pairs of deflector plates or scanning coils or typically in the final lens in the electron column. It scans in a raster fashion over a rectangular area of the sample surface. Because of the interaction of the primary electron beam and the sample surface, all the electrons lose their energy by the random scattering repetition and

absorption within a teardrop-shaped volume of the specimen known as the interaction volume, which extends from less than 100 nm to around 5 µm into the surface.

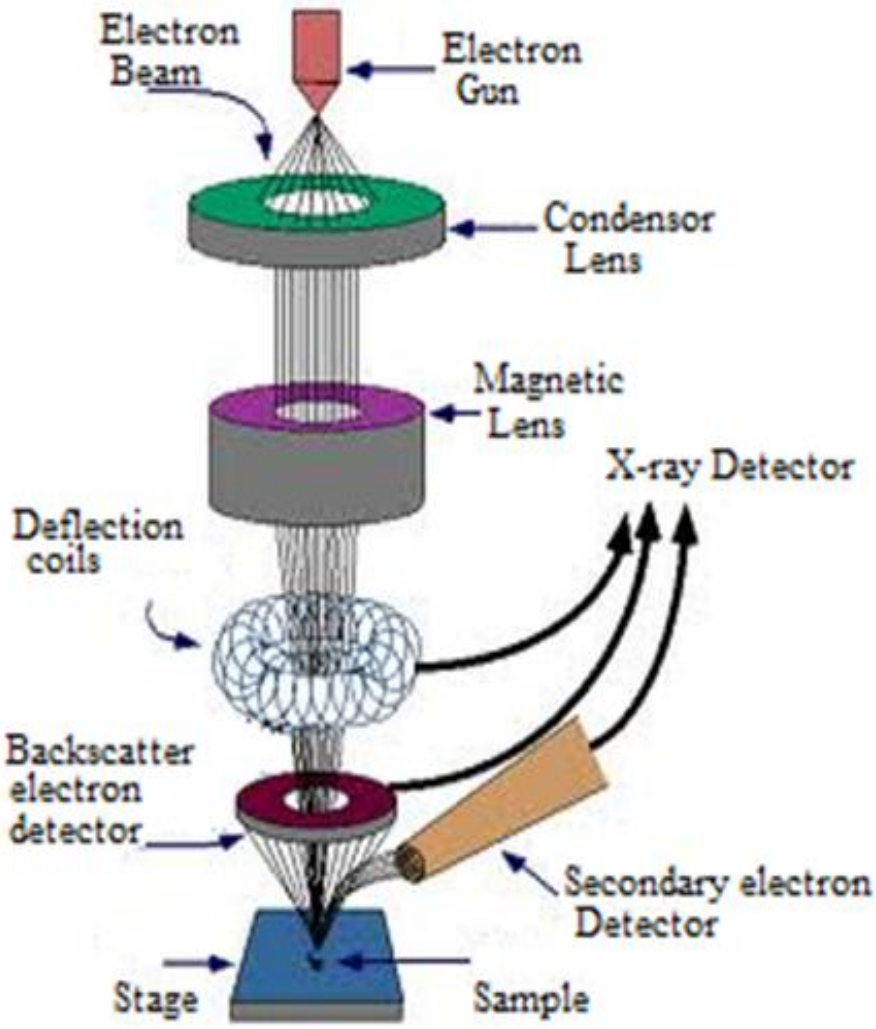

Figure: 3.3 Working of Scanning process and image formation of SEM.

The size of the interaction volume depends on the electron's landing energy, the atomic number of the specimen and the specimen's density. The specialized detectors detect the exchanging energy between the electron beam and the sample results in the reflection of high-energy electrons by elastic scattering, emission of secondary electrons by inelastic scattering and the emission of electromagnetic radiation.

The specialized detectors detected the exchanging energy between the electron beam and the sample results in the reflection of high-energy electrons by elastic scattering, emission of secondary electrons by inelastic scattering and the emission of electromagnetic radiation, each of which can be detected by specialized detectors. It can also detect the beam current which is absorbed by the specimen and it uses to create images of the distribution of specimen current. Various Electronic Amplifiers are used to amplify the signals, which are displayed on the cathode tubes as variations in brightness.

The raster scanning of the CRT display is synchronized with that of the beam on the specimen in the microscope, and the resulting image is therefore a distribution map of the intensity of the signal being emitted from the scanned area of the specimen. From a high-resolution cathode ray tube, with photography, the image may be captured, but in modern machines these images are digitally captured and displayed on a computer monitor and it can save the final images into a computer's hard disk.

3.4 LCR meter

In LCR meter (“L” represents Inductance, “C” represents Capacitance and “R” represents Resistance) is a piece of electronic test equipment which is used to measure the inductance, capacitance and resistance of a component. These quantities are not directly measured in the usual version of the instrument but these determined from the measurement of impedance. The necessary calculations are, however, incorporated in the instrument's circuitry; the meter reads L, C and R directly with no human calculation required.

Figure 3.4 represents the PM 6306 LCR meter used for dielectric measurements which is the most flexible RCL meter and allows testing with any frequency up to 1 MHz. The AC and DC test voltages are continuously adjustable and the instrument offers a built-in contact check to ensure optimum connection. With these capabilities, you can handle a wider variety of components and under more realistic test conditions.

Figure: 3.4. Fluke PM6306 programmable automatic LCR meter.

3.5 Ferroelectric Hysteresis Measurement

Hysteresis is a phenomenon that is present in all piezoelectric materials and the existence of a hysteresis loop (P-E) has been considered as evidence towards establishing that a material is ferroelectric. Hysteretic behavior is due to the lossy nature of the ceramic where the current trails the applied voltage by an angle related to the loss tangent of the material. The polarization P is a double-valued function of the externally applied electric field E. If a small electric field is first applied, only a linear relationship between P and E exists because domains stay in their initial configuration. As the electric field strength increases, the domains, whose polarization direction is opposite to the field will be switched. Consequently, the polarization increases significantly with increasing E until all of the domains are aligned in the field direction. This state is called the state of saturation.

Theoretically, this state of saturation polarization should correspond to a single domain state of the crystal. When the field is decreased to zero, the polarization does not return back to zero. Rather, the domains remain aligned, and the crystal exhibit a remnant polarization P_r. The strength of the field necessary to reduce the polarization to zero is called the coercive field E_c. Further increase of the field in the opposite direction will cause a complete alignment of the dipole domains in this opposite direction. Finally, by reversing the field once again, the process can be repeated. To characterize the amount of hysteresis in a ceramic, a sinusoidal voltage is applied to the device and the displacement is recorded. By plotting the displacement vs. driving voltage the hysteretic behavior of the ceramic can be observed.

Experimentally, Ferroelectric hysteresis loops can be measured using a Sawyer-Tower circuit or a modified version of it, applying an a.c. field and can be observed on the screen of an oscilloscope. The circuit is shown schematically in Figure.3.5

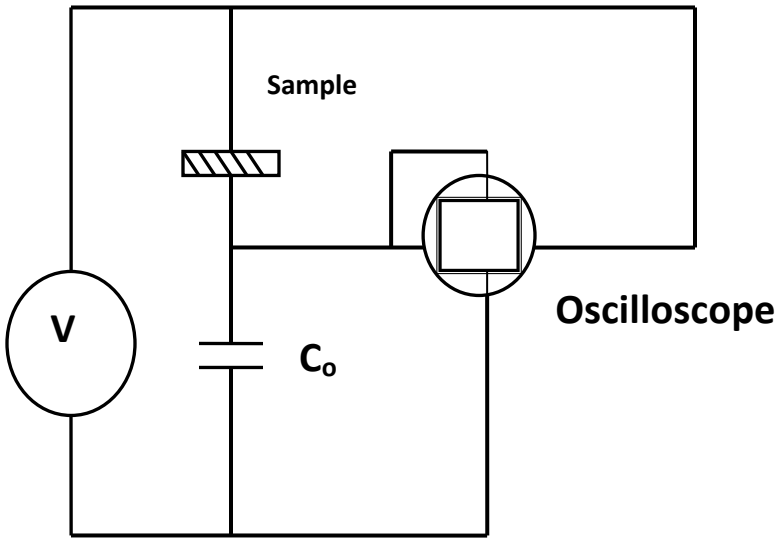

Figure: 3.5. Modified Sawyer-Tower Circuits

Horizontal axis uses the voltage across the sample and a quantity which is proportional to the field across the sample is plotted on this axis. The resulting charge stored on the sample is determined by means of a large reference capacitor C_0 placed in series with the sample. In this configuration, the voltage across C_0 is proportional to the polarization of the sample. An electrometer can be used to detect the voltage across the capacitor; by multiplying this voltage with the value of the reference capacitor, the charge across the sample results. The reference capacitor should be 100 to 1000 times the value of the capacitance of the sample. This polarization is laid across the vertical plates of the oscilloscope. This circuit not only measures the hysteresis but also quantifies the spontaneous polarization (P_s) and the coercive field (E_c). Ferroelectric measurements under present study were made using a computer controlled modified Sawyer-Tower bridge capable of automatic determination of standard P-E measurement compensation parameters.

Chapter: 4

Results and Discussion

4.1 Structural analysis

Figure 4.1 shows the XRD pattern of PLDZT (x = 0.0 and 0.03) ceramics. The patterns show formation of single rhombohedral phase. The single and sharp x-ray diffraction peaks, which are quite different in position and intensity from those of the ingredients, confirm the formation of single phase new compounds.

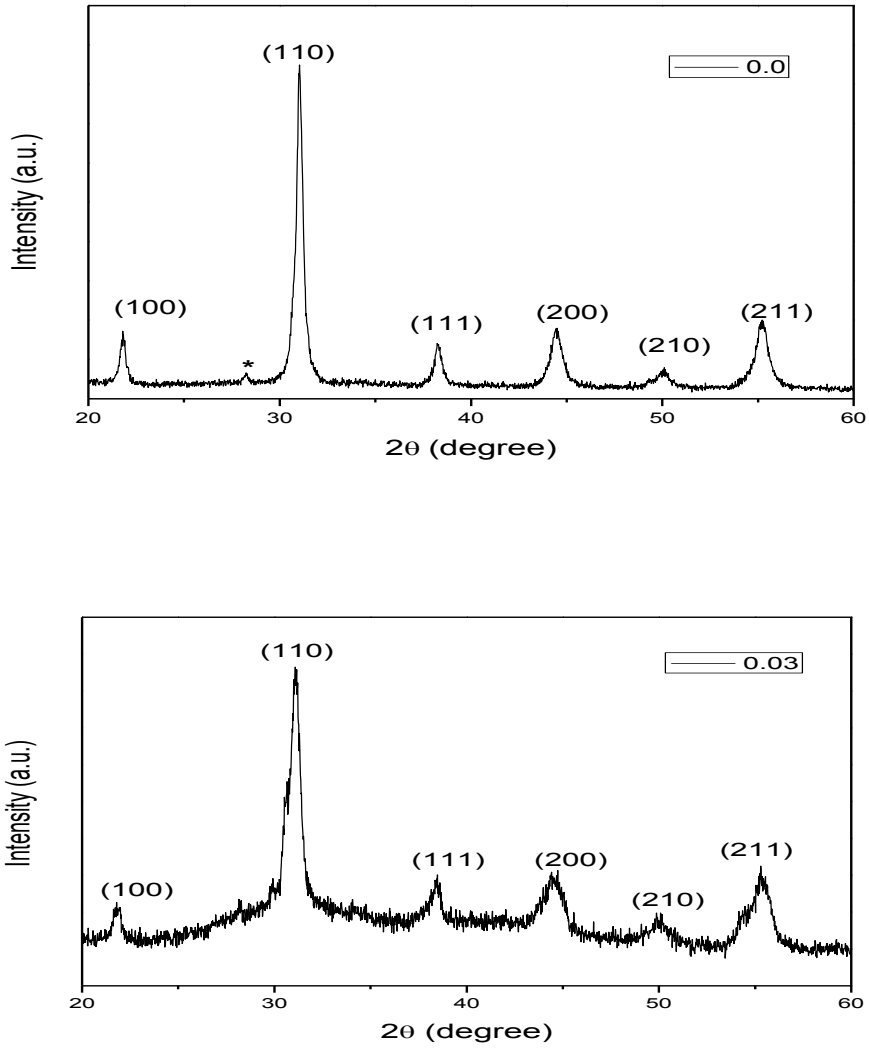

Figure: 4.1 XRD pattern Dy doped PLZT(x=0.0 and 0.03)

4.2 Microstructural analysis

The surface microstructure of the sintered Dy doped (x=0.0 and 0.03) PLZT samples observed by FE-SEM are shown in figure 4.2. Well developed and single-shaped grains are observed in both the compositions, which confirm the formation of a single phase in both the samples. PLDZT, x = 0.00 samples, shows high porosity which is observed to decrease with the doping of Dy.

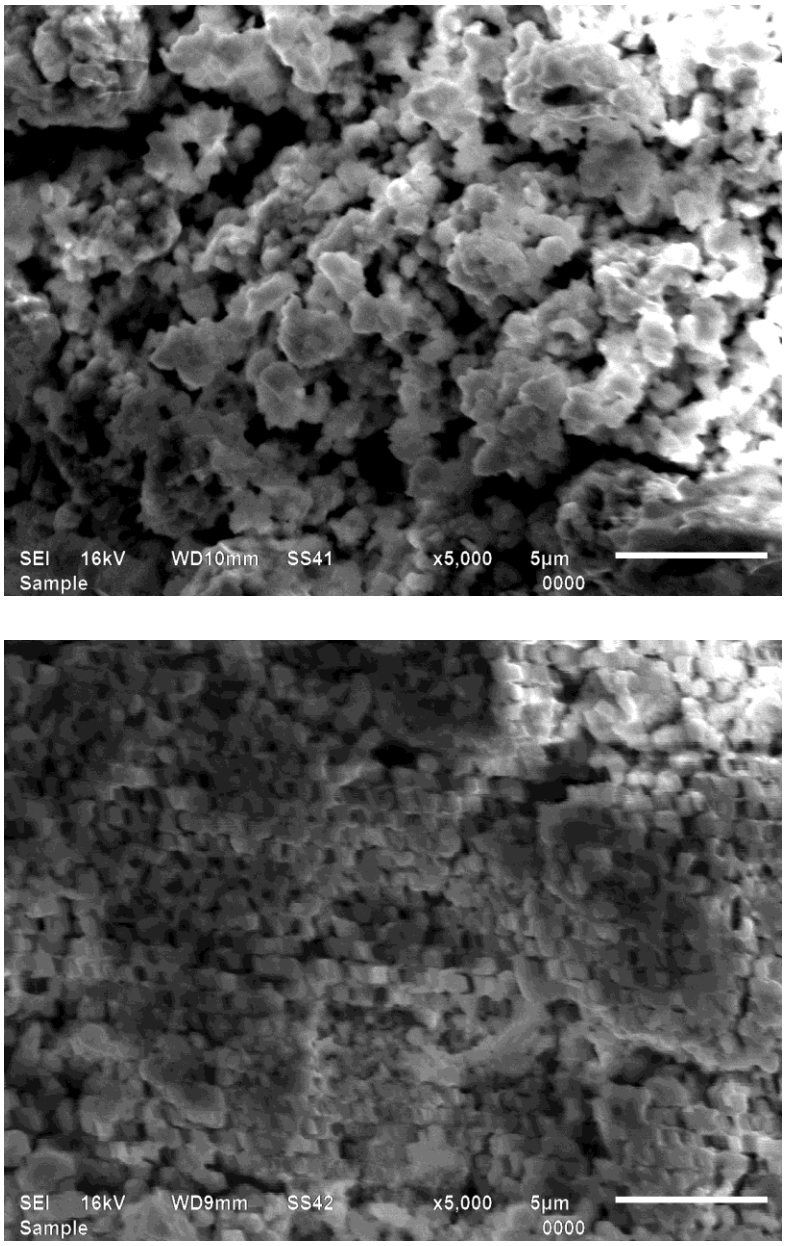

Figure: 4.2. Microstructure of the sintered Dy doped (x=0.0 and 0.03) PLZT samples.

4.3 Dielectric properties

Figures 4.3 shows the variation of the dielectric constant with temperature for Dy (x=0.0, 0.03) doped PLZT compositions at various frequencies 100Hz, 1 kHz, 10 kHz, 100 kHz and 1MHz. Here, the dielectric constant increases gradually with the increase in temperature up to transition temperature (T_c) and then decrease with further increase in temperature.

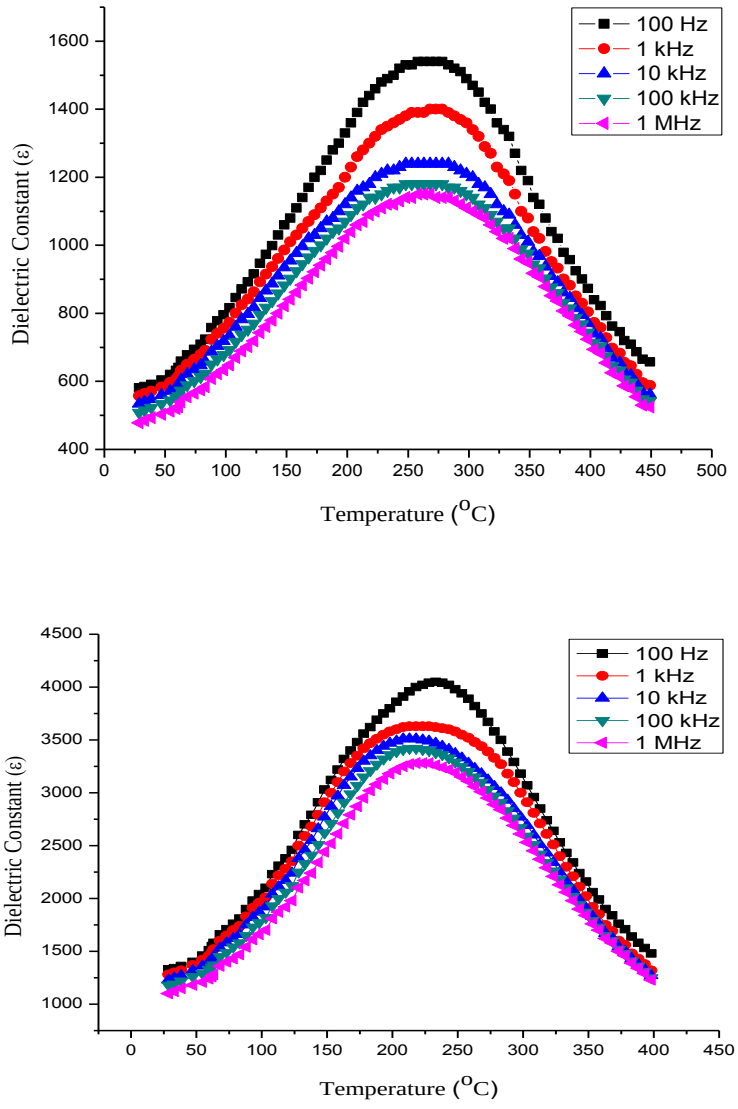

Figure: 4.3. Variation of the dielectric constant as the function of temperature for Dy(x=0.0 and 0.03) doped PLZT compositions at various frequencies 100Hz, 1 kHz, 10 kHz,100 kHz and 1MHz.

The region around the dielectric peak is broadened. The broadening and diffuseness of the peak occurs mainly due to compositional fluctuation and/or substitution disordering in the arrangement of cations in one or more crystallographic sites of the Dy doped PLZT structure. The value of peak dielectric permittivity (ε_r) increases with increase of concentration of Dy.

The transitional temperature (T_c) was found to shift towards lower temperature by 40^0C with Dy concentration from x=0.0 to 0.03.

Dy doped PLZT can be considered as disordered ferroelectric system where electric dipoles, Dy ion and intrinsic defects such as oxygen and Pb vacancies act as source of random electric field distributions which reduces T_c.

Further features of Ferro- to paraelectric phase transition of different PLDZT samples were closely analyzed. Normally ferroelectric materials are well known to follow the permittivity versus temperature dependence described by Curie-Weiss law.

$$\varepsilon = C/(T-T_0) \quad \ldots \quad [4.1]$$

where C is the Curie-Weiss constant and T_0 is Curie temperature.

From theory T_0 is expected to be less than (first order transition) or equal to (second order transition) the transition temperature T_c. An example of such a process for PLDZT (x=0.0 and 0.03) sample is shown figure 4.4, in term of $1/\varepsilon$ versus temperature graph.

The value of Curie Weiss temperature was found to be $T_0=215^0$C, while $T_c=268^0$C for x=0.0 and $T_0=202^0$C, while $T_c=233^0$C for x=0.03.

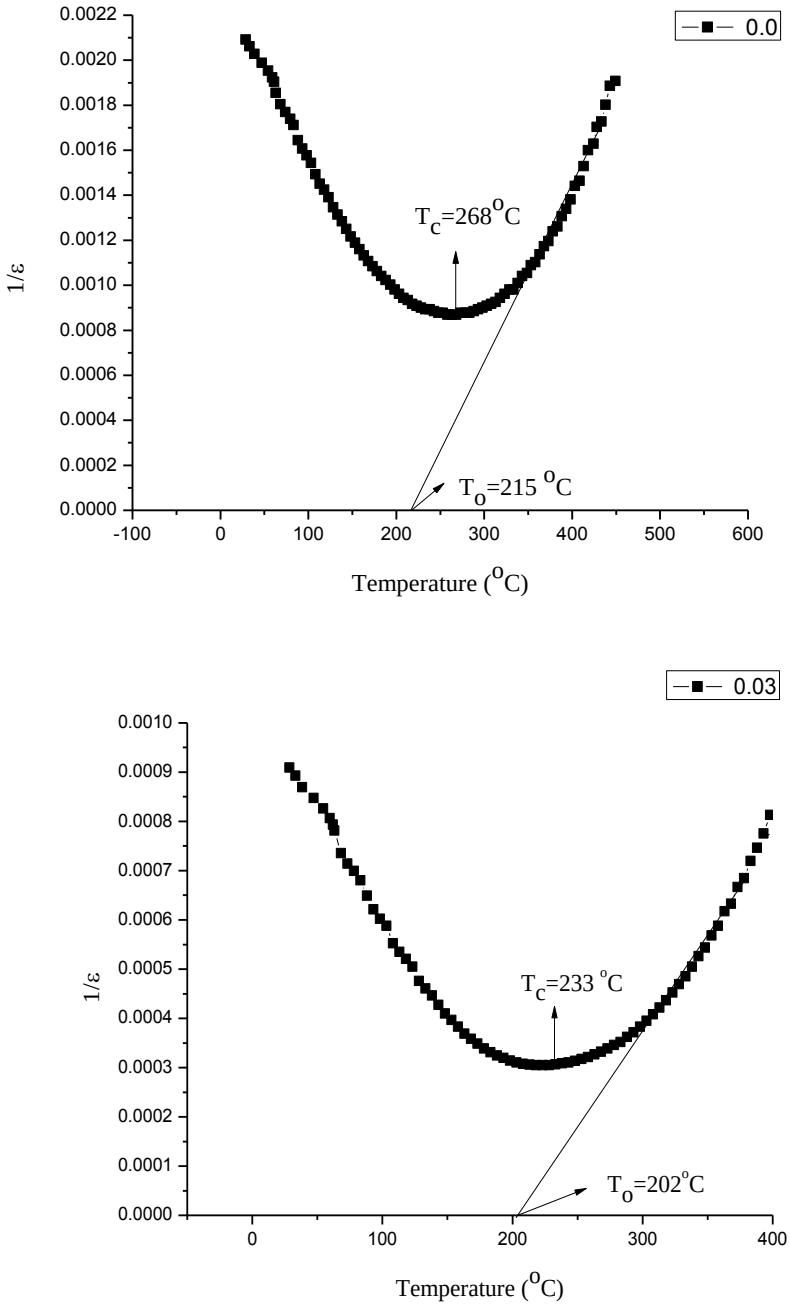

Figure: 4.4. Variation of the 1/ε as a function of temperature for Dy(x=0.0 and 0.03) doped PLZT compositions.

Deviation of Curie Weiss law is typical characteristic of ferroelectric materials exhibiting a diffusion phase transition (DPT), in the sense that their ε verses temperature spectra involves broad peak rather than sharp peak. In the literature the appearance of this diffuseness is generally argued in terms of variation in local composition giving rise to distinct micro regions, each of which has slightly different Curie points for its Ferro-paraelectric phase transitions [39, 41]. According to Smolenskii and Isupov the DPT should be described by quadratic relation [39-41].

$$1/\varepsilon = 1/\varepsilon_{max} + (T-T_c) / (2\,\varepsilon_{max}\delta^2) \quad \ldots \quad [4.2]$$

where parameter δ is called diffuse coefficient, characterizing the diffuseness of phase transition. The qualitative assessment of the diffusivity (γ) of the broadened peaks in the paraelectric phase was evaluated using the expression $(1/\varepsilon-1/\varepsilon_{max})$ versus $(T-T_c)^{\gamma}$ [42].

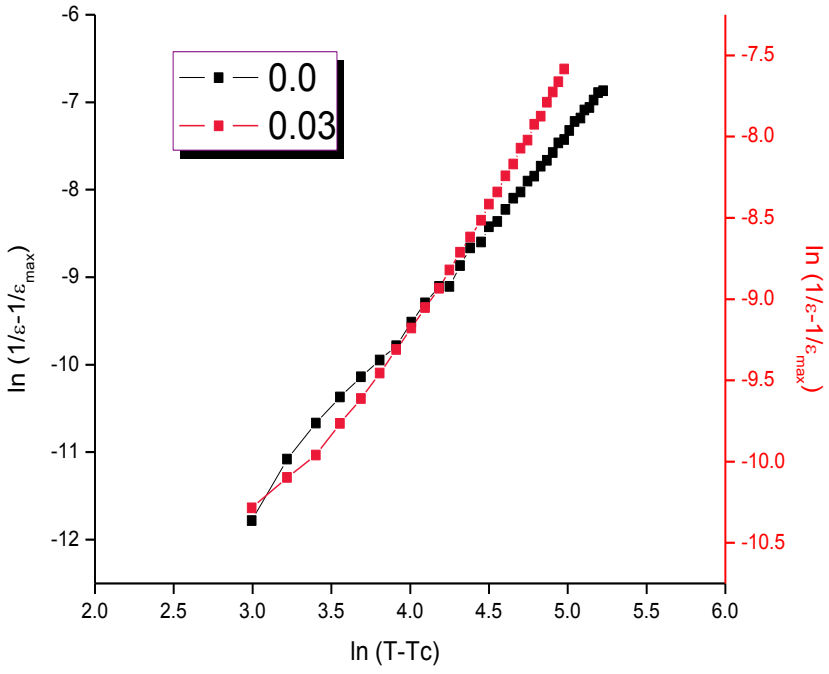

Figure: 4.5. Variation of $\ln(1/\varepsilon-1/\varepsilon_{max})$ with ln(T-Tc) at 1 MHz.

The values of γ for the all compositions was extracted from the plot of $(1/\varepsilon-1/\varepsilon_{max})$ versus $(T-T_c)$ by fitting a straight line equation. The value of γ was found to be between 1 (normal curie Weiss behavior) and 2 (completely disordered), which further confirmed the diffuse phase transition in the material.

The ac electrical conductivity for all the samples was calculated from the conductivity relation

$$\sigma=\omega\varepsilon\varepsilon_o\tan\delta \qquad \ldots [4.3]$$

where ε_o is the vacuum dielectric permittivity and ω is the angular frequency. An anomaly (a change in slope) was observed near the transition temperature T_c for all the compositions of PLDZT.

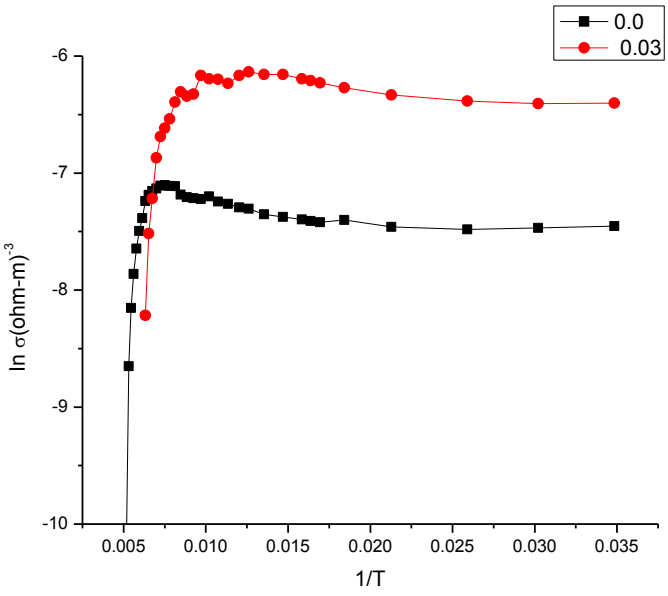

Figure: 4.6. Variation of ln σ as a function of inverse of absolute temperature (1/T) of PLDZT at 1MHz

S

4.4 Ferroelectric Properties

Figure 4.7 shows room temperature P-E loops for PLZT samples. The loops confirm the ferroelectric behavior. The figure clearly indicates increase in remnant polarization P_r from 2.24μC/cm^2 for x=0.0 to 4.72 μC/cm^2 for x=0.03, coercive field remaining the same.

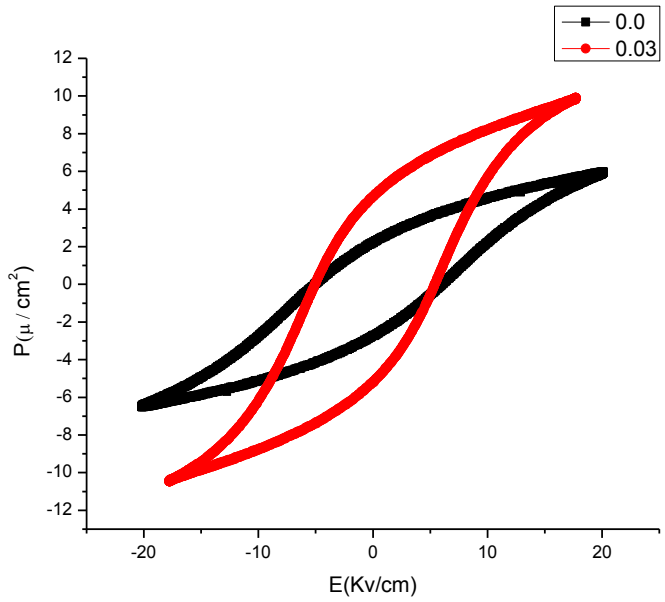

Figure: 4.7. The P-E hysteresis loop for Dy doped PLZT composition at applied field E.

Conclusion and Future scope

In this thesis, we have reported the Dy doped PLZT (65/35) ceramic with composition x=0.0 and 0.03 prepared by mixed oxide method. The effect of Dy doping on structural, microstructural, dielectric and ferroelectric properties of the PLZT (65/35) system were investigated. X-ray diffraction studies confirmed the formation of a single phase structure and rhombohedral symmetry for the synthesized compound. Dielectric constant increases gradually with the increase in temperature up to transition temperature (T_c) and then decrease with further increase in temperature for both the PLDZT ceramics doping. The transitional temperature (T_c) was found to shift towards lower temperature by 40^0C with the addition of Dy. The P-E loops confirm the ferroelectric behavior.

The present work is only aimed to study the dielectric and ferroelectric behavior of synthesized compounds. One may further do the detailed impedance analysis to investigate the various contributing factors towards resistivity. More compositions could be studied to confirm the doping/substitutional effect. Magnetic measurements could be done to investigate any multiferroicity.

References

[1] J. Valasek, "Piezoelectric and applied phenomena in Rochelle salt". Physical Review 15:537(1920) and J. Valasek physical Review 17:475(1921)

[2] S. B. Lang, Sourcebook of Pyroelectricity (Gordon and Breach, New York, (1974))

[3] M. Deri, Ferroelectric Ceramics (Gordon and Breach, New York,(1969))

[4] B. T. Batthais and A. von Hippel, Phys. Rev., 73, 1378 (1948)

[5] A. von. Hippel, Rev. Modern Phys., 22, 221 (1950)

[6] B. Ruette, MS thesis, Virginia Tech (2003)

[7] R. E. Nettleton, Ferroelectrics, 1, 3, 87, 93, 111, 121,127, 207, 221 (1970)

[8] R. E. Nettleton, Ferroelectrics, 2, 5, 77, 93 (1971)

[9] W. J. Merz, Phys. Rev., 76, 1221 (1949)

[10] J. C. Burfoot, Ferroelectrics (Van Nostrand, New York, (1967))

[11] B. Jaffe, W. R. Cook Jr., and H. Jaffe, Piezoelectric Ceramics (Academic Press, London, (1971))

[12] T. F. mling, A. Schintlmeister, H. Hutter, and J. r. Fleig, J. Am. Ceram.Soc., 94 [4] 1173–1181 (2011)

[13] J.F. Scott, Ferroelectric Memories, Springer, Berlin, (2000)

[14]Md. Ahamad Mohiddon and K. L. Yadav, P hys. Status Solidi A 206, No. 7, 1606–1615 (2009)

[15] R. Rai, S. Sharma/Ceramics International 30, 1295-1299 (2004)

[16] G.H. Haertling , J. Am. Ceram. Soc 82, 797(1999)

[17] B. Jaffe, W.R. Cook, Piezoelectric Ceramics, RAN Publishers(1971)

[18] X. Dai, Z. Xu, D. Viehland, J. Am. Ceram.Soc.78, 2815 (1995)

[19] M. Hinterstein, K. A. Schoenau, J. Kling, H. Fuess and M. Knapp, J. Appl. Phys. 108, 024110 (2010)

[20] B. Jaffe, R.C. Williams, H. Jaffe, Piezoelectric Ceramics, Academic Press, London and New York,(1971)

[21] Y. Yoshikawa, K. Tsuzuki, J. Am. Ceram. Soc. 75, 2520(1992)

[22] S.E. Park,T.R. Shrout, J. Am. Ceram. Soc. 82, 1804(1997)

[23] L.E. Cross, in: N. Setter, E.L. Colla (Eds.), Ferroelectric Ceramics—Tutorial Review Theory, Processing and Applications, Birkhauser Verlag, Basel, vol. 1(1993)

[24] K. Hardtl, D. Henings, J. Am. Ceram. Soc. 55, 230(1972)

[25] S Dutta, R N P Choudary and P K Shina Synthesis and characterization of Fe^{3+} modified PLZT ferroelectrics J. Mater. Sci. Mater. Electron.14, 463–9(2003)

[26] S Shannigrahi, R N P Choudhary, H N Acharya and T P Sinha Phase transition in sol gel-derived Na-modified PLZT ceramics J. Phys. D: Appl. Phys. 32, 1539–47(1999)

[27] K L Yadav and R N P Choudhary Structural and electrical properties of PZT (La, K) ceramics Mater. Lett.16, 291–4(1993)

[28] J Ray, P Hing and R N P Chowdary Diffuse phase transition in sol–gel-prepared modified Pb(La,Cs)(Zr,Ti)O3Mater. Lett.51, 434–43(2001)

[29] S Dutta, R N P Choudhary and P K Sinha Structural, electrical and electromechanical sensing properties of bi-modified PLZT ceramics J. Mater. Sci. Mater. Electron.15, 685–93(2004)

[30] Md. A. Mohiddon and K. L. Yadav , IEEE Transactions on Dielectrics and Electrical Insulation Vol. 15, No. 5; October (2008)

[31] K Rajni, S Sharma and T C Goel Effect of rare earth europium substitution on the microstructure, dielectric, ferroelectric and pyroelectric properties of PZT ceramics J. Electroceram. 14, 113–8(2005)

[32] S Dutta, R N P Choudhary and P K Sinha Impedance spectroscopy studies on Fe^{3+} ion modified PLZT ceramics Ceram. Int. 33, 13–20(2007)

[33] K Ramam and M Lopez Effect of acceptor and donor dopants on ferroelectric and piezoelectric properties of lead zirconium titanate ceramic Phys. Status Solidi a 15, 3852–60(2006)

[34] K H Hardtl Defect structure of PLZT doped with Mn, Fe and Al J. Am. Ceram. Soc. 64, 283–8(1981)

[35] K H Hardtl and D Hennings Distribution of A-site and B-site vacancies in (Pb, La) (Ti, Zr)O_3 ceramics J. Am. Ceram. Soc.55, 230–1(1972)

[36] R. Rai, S. Sharma/Ceramics International 30, 1295-1299(2004)

[37] Soma Dutta, R.N.P. Choudhary, P.K. Sinha, journal of material science: material in electronics 15,685-693(2004)

[38] C.D.E. Lakeman and D.A. Payne, J. Am. Ceram. Soc. 75, 3091(1992)